Interkingdom competition for Fe(III) revealed by a synthetic lethal interaction between *Caenorhabditis elegans* mitochondrial electron transport and *Escherichia coli* siderophore iron release mutations

J. Amaranath Govindan, Elamparithi Jayamani, and Gary Ruvkun*

Department of Molecular Biology, Massachusetts General Hospital, Boston, MA 02114, USA

Department of Genetics, Harvard Medical School, Boston, MA 02115, USA

*Corresponding author

Correspondence: ruvkun@molbio.mgh.harvard.edu

Abstract

C. elegans consumes bacteria which can supply essential vitamins and cofactors especially for mitochondrial functions ancestrally related to bacteria. Therefore, we screened the Keio *E. coli* knockout library for mutations that induce a *C. elegans* mitochondrial damage response gene. We identified 45 *E. coli* mutations that induce a the *C. elegans hsp-6::gfp* response gene. Surprisingly, four of these *E. coli* mutations that disrupt the import or removal of iron from the bacterial siderophore enterobactin were lethal in combination with *C. elegans* mutations that disrupt particular iron-sulfur proteins of the electron transport chain. Bacterial mutations that fail to synthesize enterobactin are not synthetic lethal with these *C. elegans* mitochondrial mutants; it is the enterobactin-iron complex that is lethal in combination with the *C. elegans* mitochondrial mutations. Antioxidants suppress this inviability, suggesting that reactive oxygen species (ROS) are produced by the mutant mitochondria in combination with the bacterial enterobactin-iron complex.

Keyword: *C. elegans*, *E. coli*, micronutrients, diet, reactive oxygen species, iron, siderophore, metabolism

Introduction

Caenorhabditis elegans, like many nematode species, consumes bacteria which supplies many nutritional needs. *C. elegans* in the laboratory consumes *E. coli*, but in its natural habitat of rotting fruit, hundreds of bacterial species are consumed by *Caenorhabditis elegans* (Félix and Braendle, 2010; Samuel et al., 2016). These diverse bacteria supply micronutrients to the animal such as vitamins and cofactors. The bacterial supply of such cofactors is so dependable that *C. elegans* is a heme auxotroph fully dependent on the bacteria it consumes to acquire this cofactor for many mitochondrial proteins in the electron transport chain (Sinclair and Hamza, 2015). Because many of the eukaryotic nuclearly-encoded proteins that localize to the mitochondria share a common ancestor with bacteria, we reasoned that other bacterial gene pathways that animals may depend upon may function for mitochondrial biogenesis or function. For example, *E. coli* mutations in the electron transport chain cytochrome *bo* terminal oxidase A gene *cyoA* cause induction of a *C. elegans* mitochondrial unfolded protein response gene, *hsp-6,* in wild type *C. elegans* (Govindan et al., 2015b). Other bacterial biosynthetic pathways on which the mitochondrion may still depend could be discovered using an animal reporter gene for mitochondrial dysfunction and a comprehensive bacterial collection of mutations. Therefore, we conducted a genome wide screen for *E. coli* mutations that induce the UPR^{mt} or affect the viability or growth of *C. elegans*. In this screen, we identified mutations in 45 *E. coli* genes out of more than 4000 *E. coli* gene disruptions tested that strongly activate the mitochondrial unfolded protein response gene, *hsp-6;* 24 of these 45 mutations also slow *C. elegans* growth. Because each of the 45 *E. coli* mutations induce a mitochondrial stress response, we tested for genetic interactions between each of these *E. coli* mutations and a set of *C. elegans* mitochondrial mutant strains. Particular *E. coli* mutations that affect the import of the iron siderophore enterobactin into the cytoplasm of *E. coli* or the retrieval of iron in the bacterial cytoplasm from the imported enterobactin bound to iron showed a dramatic synthetic lethality with weak alleles of *C. elegans* mitochondrial electron transport chain components which when grown on wild type bacteria are very healthy. Because Fe(III) is insoluble in aerobic environments, bacteria produce siderophores to retrieve Fe(III). Enterobactin binds Fe(III) with a Km of 10^{-39} M; the enterobactin bound to Fe(III) is then retrieved from outside of the cell or periplasm by specific *E. coli*

enterobactin::Fe receptors and the tightly bound Fe(III) is removed from enterobactin in the bacterial cytoplasm by a dedicated enterobactin esterase (Fischbach et al., 2006). But *E. coli* mutations that disrupt enterobactin biosynthesis genes were not synthetic lethal with *C. elegans* mitochondrial mutants. In fact, *E. coli* double mutants defective for both enterobactin synthesis and enterobactin import, or for both enterobactin synthesis and Fe(III) removal were no longer synthetic lethal with the *C. elegans* mitochondrial mutants. Thus, the production of enterobactin and a failure to remove the covalently bound iron from enterobactin is required for the toxic interaction between siderophore uptake or esterase mutant *E. coli* and *C. elegans* mitochondrial mutants. Antioxidants such as ascorbic acid or resveratrol also strongly suppressed the inviability of *C. elegans* mitochondrial mutants grown on the *E. coli* enterobactin siderophore utilization or import mutants. We hypothesize that ROS produced by *C. elegans* mitochondrial mutations when combined with ferric-chelated enterobactin to induce increased ROS, which leads to lethality. These data point to ROS as a possible interkingdom communication channel between the microbiome and the microbial-derived endosymbiont of eukaryotes, the mitochondrion.

Results

To systematically identify bacterial mutations that may affect mitochondrial function, we fed wild type *C. elegans* carrying a mitochondrial unfolded protein response chaperone gene *hsp-6::gfp* with individual bacterial mutant strains from the *E. coli* Keio collection library and screened for *E. coli* mutations that induce the mitochondrial unfolded protein response (UPR^{mt}) and/or slow *C. elegans* development. The Keio library is ~4000 single-gene in-frame insertions of a kanamycin resistance cassette in the *E. coli* K12 BW25113 background (Baba et al., 2006). *C. elegans hsp-6* encodes a mitochondrial matrix HSP70 chaperone that is specifically up-regulated by mutations or drugs that impair mitochondrial function and is a standard marker for the UPR^{mt} (Yoneda et al., 2004). We inoculated each of the 4000 Keio collection E. coli strains individually on the surface of an agar NGM *C. elegans*/E coli growth agar, added about 100 larval stage one wild type *C. elegans* carrying *hsp-6::GFP* and screened for induction of *hsp-6::GFP* using a dissecting scope fluorescence microscope. We also screened the same wells for slower than normal growth of the *C. elegans* strain. We identified 45 mutant

E. coli strains that robustly induced *hsp-6::gfp* (Table S1, Figure S1 and S2). In the same screening wells observed the next day, we screened the same *E. coli* mutants again for a delay in *C. elegans* rate of development from larval stage one to adulthood. Twenty-four of these 45 *E. coli* mutants also slowed wild type *C. elegans* growth (Table 1). All 24 of the *E. coli* mutants that cause growth delay also were retrieved in the set of 45 *E. coli* mutants that activated *C. elegans hsp-6::gfp*, suggesting that mitochondrial dysfunction is a major axis of bacterial/host nutritional interaction (Table 1). Surprisingly, none of the ~4000 viable *E. coli* Keio mutants that were screened failed to supply some essential micronutrient or macronutrient or produced a toxin that disallowed wild type *C. elegans* growth. Thus, 45 *E. coli* mutations induce a mitochondrial stress response, and half of these also slowed wild type *C. elegans* growth, but none of the Keio mutant collection was missing any essential bacterial factor (such as heme) for *C. elegans* growth. Our screen would have easily detected such a lethal interaction. There are 303 *E. coli* Keio gene disruptions that are inviable and thus not easily tested for *C. elegans* interactions.

To verify the UPR^{mt} induction, we showed that the 45 mutant *E. coli* strains that activate *hsp-6::gfp*, also activate *hsp-60::gfp,* another marker for the UPR^{mt} (Table S1). The *C. elegans* stress response induced by the 45 *E. coli* Keio mutants is specific for mitochondria because none of the 45 bacterial mutants caused activation of *hsp-4::gfp* (Table S1), a reporter of the unfolded protein response in the endoplasmic reticulum (UPR^{er}) (Kapulkin et al., 2005). Similarly, the 45 *E. coli* Keio mutants did not activate *pgp-5::gfp* (Table S1), a reporter of a translational stress response (Govindan et al., 2015a). ATFS-1 is a transcription factor required for the activation of UPR^{mt} genes, such as *hsp-6* and *hsp-60*. We tested each of the Keio *E. coli* mutants on a *C. elegans atfs-1(tm4525); hsp-60::GFP C. elegans* strain and found that all 45 bacterial mutants failed to induce the *hsp-60*::GFP UPR^{mt} in the *atfs-1(tm4525)* background (Table S1). Thus, these *E. coli* mutants activate the *C. elegans* UPR^{mt} via the expected ATFS-1 transcription factor.

Because all of the *E. coli* mutants that slowed growth induce the mitochondrial-unfolded response, and some are implicated in the *E. coli* electron transport chain, we examined whether any of these *E. coli* mutants strongly interact with *C. elegans* mutations in nuclear-encoded mitochondrial

proteins. Previous *C. elegans* RNAi screens have shown that many mitochondrial gene inactivations are lethal (Rea et al., 2007). However, viable reduction-of-function mutants have been characterized (van der Bliek et al., 2017). We tested a viable *spg-7(ad2249)* mutant (Zubovych et al., 2010). *spg-7* encodes the human homolog of AFG3L2, a conserved m-AAA metalloprotease that processes particular proteins and protein complexes in the mitochondria (Zubovych et al., 2010). Although feeding many of the 45 Keio collection *E. coli* mutants caused developmental delay in *spg-7(ad2249)*, four of the 44 Keio mutants caused a dramatic arrest phenotype in *spg-7(ad2249)*: *Δfes::kan*, *ΔfepD::kan*, *ΔfepG::kan*, *ΔfepC::kan* mutants (Table 1). For example, *Δfes::kan* feeding induces a highly penetrant very dramatic developmental arrest with *C. elegans spg-7(ad2249)* while wildtype *C. elegans* fed on *Δfes::kan* are grow normally (Figure 1A). Based on the morphological features, animal size measurements, and the germline development stage, *Δfes::kan* feeding in *spg-7(ad2249)* mutant causes an larval stage one (L1) arrest (Figure S3A-C). Each of these *E. coli* genes that cause a synthetic arrest with C. elegans mitochondrial mutant strains mediates steps in the retrieval of iron from the *E. coli* siderophore enterobactin. Enterobactin is a high-affinity iron siderophore produced by many gram-negative bacteria, including *E. coli* (Fischbach et al., 2006; Raymond et al., 2003). *E. coli* produce enterobactin under iron deficiency via the proteins encoded by the *entCDEBAH* operon (Figure 1B-C). Enterobactin is secreted into the environment, the soil or in a cell, where it binds to iron, forming a complex which is imported into *E. coli* through the transporters located in the bacterial outer membrane (Raymond et al., 2003) (Figure 1C). The ferric-enterobactin complex is transported into the cytoplasm via the *fepDGC* ATP-binding cassette transporter (Pierce and Earhart, 1986; Shea and McIntosh, 1991). FepB encodes a periplasmic protein that binds ferric enterobactin and directs it to inner membrane transporters, FepD and FepG, which pump it into the bacterial cytoplasm. FepC assists FepD and FepG in transporting ferric enterobactin from the periplasm into the cytoplasm (Figure 1C) (Guerinot, 1994). Fes encodes enterobactin esterase that catalyzes the hydrolysis of both enterobactin and ferric enterobactin. In the *E. coli* cytoplasm, Fes hydrolyses enterobactin to release iron and linearized 2,3-dihydroxy-N-benzoyl-L-serine trimer as well as the dimer and monomer (Figure 1C) (Greenwood and Luke, 1978; Langman et al., 1972; O'Brien et al., 1971). Genetic disruption of E. coli *fes* causes accumulation of the unhydrolyzed

ferric enterobactin in the bacterial cytoplasm (Brickman and McIntosh, 1992; Winkelmann et al., 1994) whereas genetic disruption fepDGC causes accumulation of the ferric enterobactin in the *E. coli* periplasm where the cytoplasmic Fes esterase cannot release iron from its nearly covalent bond in ferric enterobactin (Pierce and Earhart, 1986; Shea and McIntosh, 1991) (Figure S4A). This complex enterobactin synthesis and import biology is not parochial to *E. coli*: siderophores related to enterobactin are used across bacterial phylogeny, and the hijacking of iron-loaded siderophores produced by one species and taken up by another bacterial species is a key feature of the iron competition landscape.

To determine whether other *E. coli* genes required for enterobactin production cause the dramatic L1-synthetic larval arrest in the *spg-7 C. elegans* mitochondrial mutant, we tested each of the *E. coli* enterobactin pathway gene mutants on the *C. elegans spg-7* mutant. Feeding *C. elegans spg-7(ad2249)* mutants on *⊿entC::kan*, *⊿entD::kan*, *⊿entE::kan*, *⊿entB::kan*, *⊿entA::kan*, *⊿entH::kan,* which are defective in the production of enterobactin, does not cause L1-larval arrest (Table 2). This suggests that it is not lack of enterobactin or *E. coli* iron starvation that causes developmental arrest in the *C. elegans spg-7* mitochondrial mutant but it is the accumulation of iron-chelated enterobactin in the cytoplasm or periplasm of *E. coli* or iron-chelated enterobactin that is transported from the *E. coli* to the *C. elegans* cells with electron transport mutations that causes arrest of the *C. elegans* mitochondrial mutant.

To determine whether the L1 larval arrest caused by feeding *⊿fes::kan* mutant is specific for *spg-7(ad2249)* mutant or a more generalized phenotype of many *C. elegans* mitochondrial mutants, we tested other viable reduction-of-function *C. elegans* mitochondrial mutants (Table 3). *C. elegans nduf-7(et19)*, *isp-1(qm150)*, and *clk-1(qm30)* mutant animals grown on the *E. coli ⊿fes::kan* mutant also dramatically arrest as L1 larvae (Table 3; Figure S5) while particular other *C. elegans* mitochondrial mutants including *gas-1(fc21)*, *nduf-2.2(ok2397)*, *nuo-6(qm200)*, *mev-1(kn1)*, and *ucr-2.3(pk732)* did not arrest when grown on the *E. coli ⊿fes::kan* mutant (Table 3; Figure S5). *nduf-7(et19)* is a partial loss-of-function mutation in *nduf-7* (NADH-ubiquinone oxidoreductase Fe-S), a subunit of the mitochondrial electron transport chain complex I (Rauthan et al., 2015; van der Bliek et al., 2017). *nduf-7(et19)* mutant animals strongly activate UPR^{mt}, have a reduced respiration rate and longer lifespan (Rauthan et al., 2015). *isp-1* encodes a Rieske iron sulphur protein (ISP) that functions in the cytochrome b-c1 complex

III subunit of the mitochondrial respiratory chain (van der Bliek et al., 2017). *isp-1(qm150)* mutants have lower oxygen consumption, decreased ROS production, and increased lifespan (Feng et al., 2001). *clk-1* encodes an ortholog of the highly conserved demethoxyubiquinone (DMQ) hydroxylase that is necessary for ubiquinone biosynthesis (van der Bliek et al., 2017). Mutations in *C. elegans clk-1* causes slow development, reduced respiration, and increased lifespan when grown on an *E. coli* strain that is competent to produce bacterial ubiquinone that is identical except for a shorter isoprenoid chain that localizes this electron carrier to the membrane (Felkai et al., 1999).

Because *spg-7*, *nduf-7*, *isp-1*, and *clk-1* mediate distinct steps in mitochondrial respiratory pathways, the arrest induced by feeding mitochondrial mutants on *E. coli ⊿fes::kan* mutant is likely due to a toxic interaction between the mitochondrial homeostasis induction (one aspect of which is *hsp-6* expression) induced by the *spg-7*, *nduf-7*, *isp-1*, and *clk-1* mutations (but not by the *gas-1(fc21)*, *nduf-2.2(ok2397)*, *nuo-6(qm200)*, *mev-1(kn1)*, and *ucr-2.3(pk732)* mutations) and the iron toxicity caused by *E. coli* enterobactin mutants (Table 3).

Why do mutations that affect enterobactin-iron uptake or utilization but not enterobactin production cause developmental arrest in combination with particular *C. elegans* mitochondrial mutations? Our hypothesis is that the *E. coli* mutants that carry ferric enterobactin, but not *E. coli* mutants that make no enterobactin, are toxic for animals with the *spg-7*, *nduf-7*, *isp-1*, and *clk-1* mitochondrial dysfunctions. Inactivation of *fes* causes accumulation of the unhydrolyzed ferric enterobactin in the *E. coli* cytoplasm (Brickman and McIntosh, 1992; Winkelmann et al., 1994) whereas inactivation in FepDGC causes accumulation of the ferric enterobactin in the *E. coli* periplasm (Pierce and Earhart, 1986; Shea and McIntosh, 1991) which is inaccessible for cytoplasmic Fes to act upon (Figure S4A). As *C. elegans* consumes the Fes or Fep mutant *E. coli*, the ferric enterobactin may be unaltered by *C. elegans* esterases, which may not recognize this nearly covalent iron chelation. This ferric enterobactin may be transported into *C. elegans* cells, where if mitochondria are defective, perhaps producing ROS (see Discussion), this ferric enterobactin is now toxic.

fes is in an operon with *ybdZ* and *entF*, which are also involved in enterobactin biosynthesis. Because bacterial insertion drug resistant cassette mutations in one gene in the operon are often polar

on downstream genes, we excised the Keio collection antibiotic resistance cassette insertion in *⊿fes::kan* to create an in-frame non-polar deletion allele of the single *fes* gene in the operon, which we call *⊿fes*. Feeding *spg-7(ad2249)* mutant animals on *⊿fes E. coli* arrest also caused developmental arrest, suggesting that that the arrest phenotype is due to the absence of Fes protein, not polar effects on downstream genes (Figure 2A-B). To test whether the developmental arrest of the *C. elegans* mitochondrial mutants is due to ferric enterobactin, we inactivated enterobactin biosynthesis in the *⊿fes* mutant background by constructing *⊿fes entA::kan* and *⊿fes entB::kan* double mutants. While 100% of *C. elegans spg-7(ad2249)* mutants arrest when grown on *⊿fes* mutant *E. coli*, 0% of *spg-7(ad2249)* mutants arrest when grown the *⊿fes entA::kan* or *⊿fes entB::kan* double mutant *E. coli* that does not generate enterobactin and therefore does not generate ferric enterobactin (Figure S4B; Figure 2A-B). Further, to test whether ferric enterobactin is required within *E. coli* to produce the arrest in *spg-7(ad2249)* mutants, we constructed *⊿fes cirA782::kan, ⊿fes fepA::kan,* and *⊿fes fiu::kan* double mutants (Figure 2B). FepA is an outer membrane protein that binds and transports ferric enterobactin into the periplasm of *E. coli* (Fiss et al., 1982; Hollifield and Neilands, 1978). Fiu is an outer membrane protein that mediates uptake of dihydroxybenzoylserine, a breakdown product of enterobactin (Hantke, 1990). Cir is another outer membrane protein that mediates uptake of ferric-enterobactin and other breakdown products of enterobactin (Hantke, 1990). Although FepA, Fiu and CirA mediate import of ferric enterobactin into the bacterial periplasm, FepA is the major transporter necessary for the uptake of ferric enterobactin into bacterial periplasm. While 100% of *C. elegans spg-7(ad2249)* mutants arrest when grown on *⊿fes E. coli*, *⊿fes cirA::kan* or *⊿fes fiu::kan* double mutant *E. coli*, 0% of *spg-7(ad2249)* mutants arrest in the *⊿fes fepA::kan* double mutant *E. coli* (Figure 2B*).* This result suggests that blocking uptake of ferric enterobactin from the environment into the *E. coli* is sufficient to suppress the L1-larval arrest of *C. elegans* mitochondrial mutants grown on *⊿fes E. coli* mutant.

Because the *E. coli* enterobactin uptake and iron retrieval mutants activate a mitochondrial unfolded protein response even in a wild type *C. elegans* that grows at the normal rate (Table 1), we assessed the effect of these *E. coli* mutants on *C. elegans* mitochondrial morphology. The mitochondria of wildtype animals grown on wild type *E. coli* BW25113 have tubular or slightly elongated morphology,

but the mitochondria in the hypodermis of wildtype animals grown on *Δfes E. coli* are fragmented as assessed by Nonyl Acridine Orange (NAO), a membrane potential-independent mitochondrial dye (Figure 3A). We also used a transgenic strain that expresses mitochondrial outer membrane protein TOMM-20 tagged with mRFP in the body wall muscles of *C. elegans*. The mitochondrial morphology is tubular and elongated in animals grown on wild type *E. coli* BW25113 whereas wild type *C. elegans* grown on *Δfes E. coli* show a more fragmented mitochondria in the body wall muscle (Figure 3B). Consistent with the abnormal mitochondrial morphology, ATP levels are significantly reduced in wild type *C. elegans* grown on *Δfes E. coli* compared to wild type *E. coli* BW25113 (Figure 3C-D). These data show that the induction of the *hsp-6* in wild type *C. elegans* grown on the *E. coli* iron-siderophore retrieval mutants accurately reports their mitochondrial defects.

spg-7(ad2249) animals grown on gentamicin-treated or tetracycline-treated *E. coli Δfes* arrested at L1-arrest stage, showing that even non-growing bacteria could supply the toxic iron-siderophore product to a *C. elegans* mitochondrial mutant (Table S2). But ampicillin-killed *E. coli Δfes* did not arrest with *C. elegans spg-7(ad2249)* (Table S2). Tetracycline, kanamycin, and gentamicin are bacteriostatic whereas ampicillin targets cell wall biosynthesis and is bactericidal. Ampicillin may lyse the bacterial cell to release ferric enterobactin before the bacterial cell is engulfed in the *C. elegans* intestine to absorb ferric enterobactin.

To determine the relative dose of *E. coli Δfes* needed for this toxic interaction, we mixed various proportions of *E. coli Δfes* and wildtype BW25113. *C. elegans spg-7(ad2249)* grown on 50% live wildtype *E. coli* BW25113 and 50% live *E. coli Δfes*::*kan* did not arrest (Table S2). *spg-7(ad2249)* grown on 50% kanamycin-treated wildtype *E. coli* BW25113 and 50% live *E. coli Δfes::kan*, arrested as L1-larvae (Table S2). A mixture of 75% kanamycin-treated wildtype *E. coli* BW25113 and 25% live *E. coli Δfes* showed the L1-arrest (Table S2), showing that living wildtype *E. coli* BW25113 is required for the suppression of *E. coli Δfes* feeding-induced L1-arrest phenotype. Feeding *C. elegans spg-7(ad2249)* mutant animals on mixture of 1-part live *E. coli* BW25113 in 10,000 parts live *E. coli Δfes* fully suppressed the *E. coli Δfes* arrest; however, killed wildtype *E. coli* could not suppress arrest (Table S2).

Differential growth rates of wild type and *fes* mutant *E. coli* on *C. elegans* growth plates explains the potency of the interaction; after 48 hours on NGM plates the 1:10,000 dilution of *E. coli* BW25113 in *E. coli Δfes* had decreased to ~1.3:1 (Table S3). Thus, wildtype *E. coli* outgrows the *Δfes* mutants.

Mutations in *isp-1*, *nduf-7*, and *spg-7* cause increased ROS production by the mitochondria (Rauthan et al., 2015; Yang and Hekimi, 2010; Zubovych et al., 2010). Elevated ROS levels is essential for the resistance to hemiasterlin, a mitochondrial poison, of the *spg-7(ad2249)* mutant because this is suppressible by NAC (Zubovych et al., 2010). We found that *spg-7(ad2249)* animals that were grown on *Δfes E. coli* mutant, but mixed with antioxidants such as ascorbic acid, N-acetyl cysteine (NAC), resveratrol, or trolox completely suppressed the arrest caused by *E. coli* fes mutant fed to *C. elegans spg-7* (Figure 3E). The fact that several other antioxidants were able to suppress arrest suggests that ROS is the likely cause of the toxic interaction between bacterial mutants that accumulate ferric enterobactin and the *C. elegans* mitochondrial mutants. Elevated ROS in *isp-1(qm150)* contributes to its increased longevity because the longevity increase is suppressed by NAC (Yang and Hekimi, 2010). UPR^{mt} activation in the *nduf-7(et19)* is also suppressed by NAC (Rauthan et al., 2015). Consistent with this observation, we found that the L1-larval arrest induced by feeding *Δfes E. coli* to the *nduf-7(et19)* mutant is suppressible by NAC (Table S4). When we fed *C. elegans spg-7(ad2249)* animals the *E. coli Δfes* pre-grown in the presence of trans-resveratrol and washed off the trans-resveratrol, the animals arrest, suggesting that the site-of-action of the antioxidants is likely within the animals (Table S6).

Because hydrogen peroxide is one of the major forms of endogenous ROS, we monitored *in vivo* hydrogen peroxide levels of the interaction between the *E. coli Δfes* mutations and *C. elegans*, using HyPer, a peroxide-specific sensor protein. Transgenic wild type animals that express the HyPer sensor (*jrIs1*) (Back et al., 2012a) were grown either on *E. coli* BW25113 or *E. coli Δfes* and peroxide levels were measured. Endogenous peroxide levels were not significantly different between wild type *C. elegans* grown *E. coli* BW25113 or *E. coli Δfes*; however, addition of exogenous peroxide results in significantly higher peroxide levels in animals grown on *E. coli Δfes* compared to animals grown on *E. coli* BW25113 (Figure S6). We hypothesize that the exogenous peroxide interacts with ferric-enterobactin and via the Fenton reaction to generate more peroxide.

In the evolutionary “tug-of-war” for iron, animals rely on the enterobactin-binding protein Lipocalin-2 to counteract iron loss to microbes that secrete siderophores (Flo et al., 2004). Secreted lipocalin 2 sequesters the ferric-enterobactin to limit bacterial growth (Flo et al., 2004). We tested whether exogenous lipocalin-2 can suppress the arrest of *spg-7(ad2249)* grown on the *E. coli ⊿fes* mutant. We found that *spg-7(ad2249)* animals that were grown on the *E. coli ⊿fes* in the presence of 0.4µM of recombinant Mouse lipocalin-2 no longer arrest as L1-Larvae (Figure 3F).

Discussion

By screening a comprehensive collection of E. coli mutations, we found that 45 *E. coli* mutations activate a *C. elegans* mitochondrial stress response gene *hsp-6*. But surprisingly, four of these *E. coli* mutations that affect enterobactin siderophore utilization or import into the *E. coli* cytoplasm induce a dramatic inviability of multiple *C. elegans* mitochondrial mutants. These *E. coli* siderophore mutations also caused a mild disruption of mitochondrial morphology in wild type and the induction of *C. elegans hsp-6* (Figure 3A-B). But disruption of *E. coli* enterobactin biosynthesis did not cause this synthetic lethal interaction with a *C. elegans* mitochondrial mutants and could even suppress the synthetic lethality of *E. coli* mutants defective for enterobactin siderophore utilization or import into the cytoplasm, suggesting that the production of enterobactin is required for the toxic interaction between the iron loaded *E. coli* siderophore and *C. elegans* mitochondrial mutants.

We found that four of the mitochondrial mutations we tested were synthetic lethal with the enterobactin iron retrieval mutants but that the *gas-1* and *mev-1* mutants which also produce more ROS were not synthetic lethal. It may be important to the genetic interaction with the *E. coli* siderophore iron release mutations whether the ROS is generated in complex I or complex III, and how accessible it might be to the iron-loaded enterobactin. The detailed cryoEM structure of the entire animal mitochondrial ETC points to a highly intricate system of eight proteins bearing iron sulfur cluster redox centers that pass electrons with quantum mechanical precision, and efficiently couple to movements of transmembrane segments of other coupled Complex I proteins (there are 14 core proteins in complex I) to pump protons against a proton gradient (Sazanov, 2015). The many FeS clusters mediate the movement of electrons

along the many protein subunits of complex I are the likely source of ROS in the complex I mutants. Interestingly, from the set of ETC mutants that are synthetic lethal with the four *E. coli* siderophore iron retrieval mutants, *nduf-7* encodes an orthologue of human NDUFS7 (NADH:ubiquinone oxidoreductase core subunit S7) which has a 4 Fe 4 S cluster. The complex III ETC mutation *isp-1* also shows a strong synergistic interaction with the *E. coli* siderophore mutations. ISP-1 is an orthologue of human UQCRFS1 (ubiquinol-cytochrome c reductase, Rieske iron-sulfur polypeptide 1) and has a 2 iron, 2 sulfur clusters and ubiquinol-cytochrome-c reductase activity. Again, this is an iron sulfur center mutant protein that interacts with ubiquinone that shows such a strong synergy.

The *C. elegans spg-7* point mutation causes a mitochondrial defect and is strongly synthetically lethal with the *E. coli* siderophore Fe retrieval mutations. *spg-7* does not encode an ETC component, but encodes a protease that is the ortholog of the *E. coli* ftsH protease. This protease has a small number of client proteins, which includes the iron sulfur assembly factor iscS and the iron sulfur protein lpxC and fdoH. *C. elegans* mitochondrial proteins from the nuclear genome that are probable clients of SPG-7 are likely to be orthologs of the *E. coli* clients of ftsH: The *C. elegans* iron sulfur assembly factor *iscu-1* is a prime candidate for causing the iron sulfur protein defect in the ETC (Westphal et al., 2012).

Similarly, the *clk-1*/mammalian coenzymeQ7 mitochondrial 5-demethoxyubiquinone hydroxylase that is synthetic lethal with the *E. coli* siderophore iron retrieval mutants fails to synthesize ubiquinone with its normally 10 isoprene unit hydrophobic tail in *C. elegans*. This null allele is not lethal to *C. elegans* because *E. coli* ubiquinone is imported into *C. elegans* cells. But the *E. coli* ubiquinione while competent for viability has a shorter bacterial isoprene tail and causes slow growth of *C. elegans*, probably due to inefficient transfer of electrons from complex I to *E. coli* ubiquinone or from *E. coli* ubiquinone to complex III. The most likely explanation for the synergistic lethality of the *C. elegans clk-1* mutation with the *E. coli* siderophore mutations is that the efficiency of *E. coli* ubiquinone interaction with complex I or complex III is compromised so that ROS to synergize with the iron loaded siderophore is generated (Jonassen et al., 2001).

Of the ETC subunits that do not interact with the *E. coli* siderphore mutations includes *gas-1* and *mev-1*. *gas-1* is orthologous to human NDUFS2 (NADH:ubiquinone oxidoreductase core subunit S2)

does not have an iron sulfur cluster. *mev-1* is an ortholog of human SDHC (succinate dehydrogenase complex subunit C) and is a heme protein. *mev-1* is component of complex II, which does not participate in the NADH to oxygen redox/proton pumping cascade and would not be expected to generate ROS under normal redox conditions.

We propose that ROS production at particular sites in the ETC is the key to the genetic interaction with *E. coli* siderphore mutations. Such localized production of ROS may not be detectable when measuring ROS levels in extracts; but the localized ROS within complex I or III could explain the phenotype. In fact, the free radical scavenger suppression, where such small scavenger molecules may weave into Fe S clusters, is evidence that free radicals are involved.

It is important to note that all of the mitochondrial mutations used in this study are non-null point mutations. The null phenotypes for all these genes are lethal (based on gene inactivations by RNAi). Thus, the complexities of which mitochondrial mutations synergize and which do not can be interpreted based on the functions of each protein, but these interpretations are diminished by the fact that single point mutations were screened (ie, these are not null phenotypes). Still, the correlation with Fe S proteins and *E. coli* siderophore genetic interactions is striking. And the ability of antioxidants to suppress the arrest induced by *E. coli* mutants defective in enterobactin siderophore utilization or import with *C. elegans* mitochondrial mutants suggests a ROS-based mechanism for the toxicity. Because endogenous ROS production is minimal in wildtype *C. elegans*, whereas mitochondrial mutants have increased ROS production, we propose that the triggering ROS in the *C. elegans* mitochondrial mutant animals when combined with ferric-chelated enterobactin induces a much larger ROS burst via the Fenton reaction to cause toxicity to *C. elegans*. However, in wildtype *C. elegans*, since there is minimal ROS production, there is not enough ROS to initiate the Fenton reaction; thus *E. coli* enterobactin siderophore utilization or import mutants do not induce larval arrest in wild type *C. elegans*. Nevertheless, the ferric chelated enterobactin that enters the wildtype *C. elegans* does activate the mitochondrial stress response. Another possibility is that since the mitochondria in the specific mitochondrial mutants are mildly dysfunctional, adding the toxic ferric chelated enterobactin exacerbates the mitochondrial damage. Since the mitochondria of the wildtype *C. elegans* are healthier, the *E. coli*

enterobactin utilization or import mutants do not cause larval arrest in wildtype. In summary, our findings highlight the importance of gut microbial metabolites in regulating animal health through conserved mitochondrial bioenergetics pathways.

Other studies have identified the importance of iron and enterobactin in the growth rate of *C. elegans* (Qi and Han, 2018). Enterobactin binds the ATP synthase subunit ATP-1 (F0 subunit alpha, equivalent to atpA of bacteria) of mitochondrial respiratory chain (Qi and Han, 2018). Although ATP synthase is not an iron-rich protein, it does cross the same mitochondrial membrane and uses the pH gradient generated by the electron transport chain to power the ATP synthase rotary motor. The iron-rich Complex I of the ETC passes electrons along the redox gradient from NADH, eventually via Complexes III and IV to oxygen, coupling that energy to the movements of iron-sulfur and heme proteins to pump protons.

Acknowledgments

We thank members of the G.R. laboratory for helpful discussions. The work was supported by NIH Grant AG043184 (to G.R.). **Some strains were provided by the CGC, which is funded by NIH Office of Research Infrastructure Programs (P40 OD010440).**

Author contributions

J.A.G., E.J, and G.R. conceived the project. J.A.G. performed all experiments with technical help from E.J. J.A.G. analyzed all the data, made the figures, and wrote the paper. G.R. supervised the experiments and wrote the paper with the help from the other authors.

Declaration of Interests

The authors declare no competing interests.

References:

Baba, T., Ara, T., Hasegawa, M., Takai, Y., Okumura, Y., Baba, M., Datsenko, K.A., Tomita, M., Wanner, B.L., Mori, H., 2006. Construction of Escherichia coli K-12 in-frame, single-gene knockout mutants: the Keio collection. Mol Syst Biol 2, 2006–0008. doi:10.1038/msb4100050

Back, P., De Vos, W.H., Depuydt, G.G., Matthijssens, F., Vanfleteren, J.R., Braeckman, B.P., 2012a. Exploring real-time in vivo redox biology of developing and aging Caenorhabditis elegans. Free Radic. Biol. Med. 52, 850–859. doi:10.1016/j.freeradbiomed.2011.11.037

Back, P., De Vos, W.H., Depuydt, G.G., Matthijssens, F., Vanfleteren, J.R., Braeckman, B.P., 2012b. Exploring real-time in vivo redox biology of developing and aging Caenorhabditis elegans. Free Radic. Biol. Med. 52, 850–859. doi:10.1016/j.freeradbiomed.2011.11.037

Brickman, T.J., McIntosh, M.A., 1992. Overexpression and purification of ferric enterobactin esterase from Escherichia coli. Demonstration of enzymatic hydrolysis of enterobactin and its iron complex. J Biol Chem 267, 12350–12355.

Felkai, S., Ewbank, J.J., Lemieux, J., Labbé, J.C., Brown, G.G., Hekimi, S., 1999. CLK-1 controls respiration, behavior and aging in the nematode Caenorhabditis elegans. EMBO J 18, 1783–1792. doi:10.1093/emboj/18.7.1783

Feng, J., Bussière, F., Hekimi, S., 2001. Mitochondrial electron transport is a key determinant of life span in Caenorhabditis elegans. Dev. Cell 1, 633–644.

Félix, M.-A., Braendle, C., 2010. The natural history of Caenorhabditis elegans. Curr. Biol. 20, R965–9. doi:10.1016/j.cub.2010.09.050

Fischbach, M.A., Lin, H., Liu, D.R., Walsh, C.T., 2006. How pathogenic bacteria evade mammalian sabotage in the battle for iron. Nat. Chem. Biol. 2, 132–138. doi:10.1038/nchembio771

Fiss, E.H., Stanley-Samuelson, P., Neilands, J.B., 1982. Properties and proteolysis of ferric enterobactin outer membrane receptor in Escherichia coli K12. Biochemistry 21, 4517–4522.

Flo, T.H., Smith, K.D., Sato, S., Rodriguez, D.J., Holmes, M.A., Strong, R.K., Akira, S., Aderem, A., 2004. Lipocalin 2 mediates an innate immune response to bacterial infection by sequestrating iron. Nature 432, 917–921. doi:10.1038/nature03104

Govindan, J.A., Jayamani, E., Zhang, X., Breen, P., Larkins-Ford, J., Mylonakis, E., Ruvkun, G., 2015a. Lipid signalling couples translational surveillance to systemic detoxification in Caenorhabditis elegans. Nat Cell Biol 17, 1294–1303. doi:10.1038/ncb3229

Govindan, J.A., Jayamani, E., Zhang, X., Mylonakis, E., Ruvkun, G., 2015b. Dialogue between E. coli free radical pathways and the mitochondria of C. elegans. Proc Natl Acad Sci U S A. doi:10.1073/pnas.1517448112

Greenwood, K.T., Luke, R.K., 1978. Enzymatic hydrolysis of enterochelin and its iron complex in Escherichia Coli K-12. Properties of enterochelin esterase. Biochim. Biophys. Acta 525, 209–218.

Guerinot, M.L., 1994. Microbial iron transport. Annu Rev Microbiol 48, 743–772. doi:10.1146/annurev.mi.48.100194.003523

Hantke, K., 1990. Dihydroxybenzoylserine--a siderophore for E. coli. FEMS Microbiol. Lett. 55, 5–8.

Hollifield, W.C., Neilands, J.B., 1978. Ferric enterobactin transport system in Escherichia coli K-12. Extraction, assay, and specificity of the outer membrane receptor. Biochemistry 17, 1922–1928.

Jonassen, T., Larsen, P.L., Clarke, C.F., 2001. A dietary source of coenzyme Q is essential for growth of long-lived Caenorhabditis elegans clk-1 mutants. Proceedings of the National Academy of Sciences 98, 421–426. doi:10.1073/pnas.021337498

Kapulkin, W.J., Kapulkin, V., Hiester, B.G., Link, C.D., 2005. Compensatory regulation among ER chaperones in C. elegans. FEBS Lett. 579, 3063–3068. doi:10.1016/j.febslet.2005.04.062

Lagido, C., McLaggan, D., Glover, L.A., 2015. A Screenable In Vivo Assay for Mitochondrial Modulators Using Transgenic Bioluminescent Caenorhabditis elegans. J Vis Exp e53083–e53083. doi:10.3791/53083

Langman, L., Young, I.G., Frost, G.E., Rosenberg, H., Gibson, F., 1972. Enterochelin system of iron transport in Escherichia coli: mutations affecting ferric-enterochelin esterase. J Bacteriol 112, 1142–1149.

O'Brien, I.G., Cox, G.B., Gibson, F., 1971. Enterochelin hydrolysis and iron metabolism in Escherichia coli. Biochim. Biophys. Acta 237, 537–549.

Palikaras, K., Tavernarakis, N., 2016. Intracellular Assessment of ATP Levels in Caenorhabditis elegans. Bio Protoc 6. doi:10.21769/BioProtoc.2048
Pierce, J.R., Earhart, C.F., 1986. Escherichia coli K-12 envelope proteins specifically required for ferrienterobactin uptake. J Bacteriol 166, 930–936.
Qi, B., Han, M., 2018. Microbial Siderophore Enterobactin Promotes Mitochondrial Iron Uptake and Development of the Host via Interaction with ATP Synthase. Cell 175, 571–582.e11. doi:10.1016/j.cell.2018.07.032
Rauthan, M., Ranji, P., Abukar, R., Pilon, M., 2015. A Mutation in Caenorhabditis elegans NDUF-7 Activates the Mitochondrial Stress Response and Prolongs Lifespan via ROS and CED-4. G3 (Bethesda) 5, 1639–1648. doi:10.1534/g3.115.018598
Raymond, K.N., Dertz, E.A., Kim, S.S., 2003. Enterobactin: an archetype for microbial iron transport. Proceedings of the National Academy of Sciences 100, 3584–3588. doi:10.1073/pnas.0630018100
Rea, S.L., Ventura, N., Johnson, T.E., 2007. Relationship between mitochondrial electron transport chain dysfunction, development, and life extension in Caenorhabditis elegans. PLoS Biol 5, e259. doi:10.1371/journal.pbio.0050259
Samuel, B.S., Rowedder, H., Braendle, C., Félix, M.-A., Ruvkun, G., 2016. Caenorhabditis elegans responses to bacteria from its natural habitats. Proc Natl Acad Sci U S A 113, E3941–9. doi:10.1073/pnas.1607183113
Sazanov, L.A., 2015. A giant molecular proton pump: structure and mechanism of respiratory complex I. Nat. Rev. Mol. Cell Biol. 16, 375–388. doi:10.1038/nrm3997
Shea, C.M., McIntosh, M.A., 1991. Nucleotide sequence and genetic organization of the ferric enterobactin transport system: homology to other periplasmic binding protein-dependent systems in Escherichia coli. Mol Microbiol 5, 1415–1428.
Sinclair, J., Hamza, I., 2015. Lessons from bloodless worms: heme homeostasis in C. elegans. Biometals 28, 481–489. doi:10.1007/s10534-015-9841-0
van der Bliek, A.M., Sedensky, M.M., Morgan, P.G., 2017. Cell Biology of the Mitochondrion. Genetics 207, 843–871. doi:10.1534/genetics.117.300262
Westphal, K., Langklotz, S., Thomanek, N., Narberhaus, F., 2012. A trapping approach reveals novel substrates and physiological functions of the essential protease FtsH in Escherichia coli. J Biol Chem 287, 42962–42971. doi:10.1074/jbc.M112.388470
Winkelmann, G., Cansier, A., Beck, W., Jung, G., 1994. HPLC separation of enterobactin and linear 2,3-dihydroxybenzoylserine derivatives: a study on mutants of Escherichia coli defective in regulation (fur), esterase (fes) and transport (fepA). Biometals 7, 149–154.
Yang, W., Hekimi, S., 2010. A mitochondrial superoxide signal triggers increased longevity in Caenorhabditis elegans. PLoS Biol 8, e1000556–e1000556. doi:10.1371/journal.pbio.1000556
Yoneda, T., Benedetti, C., Urano, F., Clark, S.G., Harding, H.P., Ron, D., 2004. Compartment-specific perturbation of protein handling activates genes encoding mitochondrial chaperones. J. Cell. Sci. 117, 4055–4066. doi:10.1242/jcs.01275
Zubovych, I.O., Straud, S., Roth, M.G., 2010. Mitochondrial dysfunction confers resistance to multiple drugs in Caenorhabditis elegans. Mol Biol Cell 21, 956–969. doi:10.1091/mbc.E09-08-0673

Figure legends

Figure 1: *E. coli* mutations that affect enterobactin siderophore utilization or import are synthetic lethal with *C. elegans* mitochondrial mutations

A) *spg-7(ad2249)* animals grown on *Δfes::kan E. coli* arrest as L1-larvae. Scale bar, 1000μM.

B) Operon structure of genes in the enterobactin pathway

C) Diagrammatic representation of enterobactin biosynthetic pathway in *E. coli*.

Figure 2: Enterobactin is necessary for the developmental arrest phenotype of *C. elegans* mitochondrial mutants

A) *spg-7(ad2249)* animals grown on wildtype *E.coli* BW25113 develop normally while *spg-7(ad2249)* mutant grown in Δ*fes* mutant arrest as L1-larvae. In contrast, *spg-7(ad2249)* animals grown on *Δfes ΔentA::kan* double mutants develop normally. Scale bar, 1000μM.

B) Table showing suppression of the larval arrest phenotype in animals grown on *Δfes ΔentA::kan*, *Δfes ΔentB::kan*, and *Δfes ΔfepA::kan* mutants. Data from three independent trials were collected; the average of percentage of adults and the standard deviation are shown. The total number of animals counted in all the three independent trials is shown in the parentheses.

Figure 3: Mitochondrial structure and function are disrupted in wildtype animals grown on Δ*fes* mutant *E. coli*

A) Wildtype animals grown on Δ*fes* mutant *E. coli* display fragmented hypodermal mitochondrial morphology as assessed using NAO. Scale bar, 100μM.

B) Transgenic animals expressing TOMM-20::mRFP in the muscles grown on Δ*fes* mutant *E. coli* display a fragmented mitochondrial morphology. Scale bar, 100μM.

C) Animals grown on Δ*fes* mutant *E. coli* display lowered ATP levels compared to animals grown on *E.coli* BW25113 as assessed using a strain that expresses luciferase in all tissues. Unpaired t-test; *** $P< 0.001$. Mean ± s.d of n=10.

D) ATP levels in animals grown on Δ*fes* mutant *E. coli* display lowered ATP levels compared to animals grown on *E.coli* BW25113. Unpaired t-test; *** $P< 0.001$. Mean ± s.d of n=3.

E) While antioxidant treatments suppress the L1-larval arrest phenotype induced by feeding Δ*fes* mutants to *C. elegans* mitochondrial mutants, cis-resveratrol and cis-trimethoxyresveratrol fails to suppress the arrest phenotype. While trans-resveratrol and oxyresveratrol suppressed arrest, cis-resveratrol or cis-trimethoxy resveratrol did not suppress the arrest: perhaps these isomers distinguish between the free radical production surface. Data from three independent trials were collected; the average of percentage of adults and the standard deviation are shown. The total number of animals counted in all the three independent trials is shown in the parentheses.

F) Mouse lipocalin is sufficient to suppress the larval arrest phenotype of *spg-7(ad2249)* animals grown on Δ*fes* mutants. Data from three independent trials were collected; the average of percentage of adults and the standard deviation are shown. The total number of animals counted in all the three independent trials is shown in the parentheses.

Table 1: Quantification of developmental delay phenotype in wildtype background and *spg-7(ad2249)* mutant background

Synchronized L1 larval stage wildtype animal were inoculated onto NGM media plates seeded with individual Keio *E. coli* mutant strains and incubated at 20°C. The number of adult animals and the total number of animals were counted on day 3 and day 4 of feeding wildtype animals on Keio *E. coli* mutant strains. Data from three independent trials were collected; the average of percentage of adults and the standard deviation are shown. The total number of animals counted in all the three independent trials is shown in the parentheses. [a]Compared to Wildtype animals fed on BW25113 on day 3, Unpaired t-test, $P<0.0001$. [b]Since there were no adults or only few adults on these plates, the plates were scored on day 4 for the presence of adults. While there were no adults on day3, many of the wells had animals that reached adulthood on day 4. NA, Not applicable since all the animals were adults on day 3 itself. For column 4 and 5, synchronized L1 larval stage *spg-7(ad2249)* mutant were inoculated onto NGM media plates seeded with individual Keio *E. coli* mutant strains and incubated at 20°C. The number of adult animals and the total number of animals were counted on day 4 and 5 of feeding *spg-7(ad2249* animals on Keio *E. coli* mutant strains. Data from three independent trials were collected; the average of

percentage of adults and the standard deviation are shown. The total number of animals counted in all the three independent trials is shown in the parentheses.

Table 2: Feeding Ferric-Enterobactin induces developmental arrest in *C. elegans* mitochondrial mutants

Synchronized L1 larval stage wildtype or *spg-7(ad2249)* mutant were inoculated onto NGM media plates seeded with individual Keio *E. coli* mutant strains and incubated at 20°C. The number of L1-arrest animals and the total number of animals were counted on day 3.

Table 3: Table showing list of the mitochondrial mutants tested to potential interaction with Δ*fes* mutant.

Data from three independent trials were collected; the average of percentage of L1 animals and the standard deviation are shown. The total number of animals counted in all the three independent trials is shown in the parentheses.

Supplemental information

Supplemental information includes seven figures and four tables

Figure S1: Screen methodology

Individual Keio mutant *E. coli* strains were grown in individual wells of 24 well NGM agar plates, which supports bacterial growth on the surface, and the bacteria that grew on the agar surface were inoculated the next day with ~30 synchronized L1 larval stage *hsp-6::gfp* animals. Each individual well was then screened at two different time-points: 48 hours at 20°C for the Keio mutant strains that induced *hsp-6::gfp* and at 96 hours at 20°C for *E. coli* mutant strains that dramatically slowed *C. elegans* development.

Figure S2: *E. coli* mutants induce *hsp-6::gfp*

While *hsp-6::gfp* is not induced in animals grown on wildtype *E. coli* BW25113, animals grown on mutant Keio *E. coli* strains showed *hsp-6::gfp* activation.

Figure S3: Determining the arrest stage of *spg-7(ad2249)* animals grown on Δ*fes-722* mutant

A) The size and appearance of L1-larval stage wildtype or *spg-7(ad2249)* animals from egg-prep looks very similar to that of the arrested *spg-7(ad2249)* animals grown on *fes-722* mutant *E. coli* for 4 days. One-day old wildtype animals used for comparison was grown on *fes-722* mutant *E. coli* from L1-stage for 4 days. Scale bar, 100µM.

B) Quantification of the animal length in L1-larval stage wildtype or *spg-7(ad2249)* animals from egg-prep and arrested *spg-7(ad2249)* animals grown on *fes-722* mutant *E. coli* for 4 days. One-day old wildtype animals used for comparison were grown on *fes-722* mutant *E. coli* from L1-stage for 4 days. Statistical significance was determined using one-way ANOVA. **** P<0.0001. ns denotes not significantly different. The number of animals used is shown above each bar in the graph. The error bars indicate standard deviation. Data represent one out of two independent experiments.

C) Whole-mount DAPI staining of animals from L1-larval stage wildtype or *spg-7(ad2249)* animals from egg-prep and arrested *spg-7(ad2249)* animals grown on *fes-722* mutant *E. coli*. One-day old wildtype animals were used for comparison. The germline in the L1-larval stage wildtype or *spg-7(ad2249)* animals from egg-prep and arrested *spg-7(ad2249)* animals grown on *fes-722* mutant *E. coli* were not apparently visible at this stage because at this stage there are only 2 germline progenitor cells. If the arrested worms were in their L2 or L3 stages they would have apparently visible germ cells. The germline from adult wildtype animal (red box) is shown for comparison.

Figure S4: Diagrammatic representation of bacterial enterobactin content

A) Diagrammatic representation of *Δfes::kan*, *ΔfepD::kan*, *ΔfepG::kan*, *ΔfepC::kan* mutant accumulating ferric enterobactin

B) Diagrammatic representation of *Δfes* mutant accumulating ferric-enterobactin and lack of enterobactin in *Δfes ΔentA::kan* double mutants.

Figure S5: Interaction between mitochondrial mutants and Δ*fes-722* mutant

E. coli mutants cause development arrest phenotype in *nduf-7(et19)*, *isp-1(qm150)*, and *clk-1(qm30)* mutants. No development arrest phenotype was observed in *gas(fc21)* and *ucr-2.3(pk732)* mutants grown on Δ*fes-722*.

Figure S6: Measuring hydrogen peroxide levels

Endogenous hydrogen peroxide levels were not significantly different between animals grown on *E. coli* BW25113 or *Δfes-722 E. coli*; however, addition of exogenous peroxide results in significantly higher level of endogenous peroxide levels in animals grown on *Δfes-722 E. coli* compared to animals grown on *E. coli* BW25113.

Table S1: Table showing list of the hits from the keio screen for mutants that induces *hsp-6::gfp*. All these mutant were found to induce *hsp-60::gfp*. None of these mutants activated *hsp-4::gfp* or *pgp-5::gfp*.

Table S2: *spg-7(ad2249)* animals grown on Δ*fes-722* mutant *E. coli* killed with gentamicin or tetracycline arrest as L1-larvae.

Data from three independent trials were collected; the average of percentage of L1 animals and the standard deviation are shown. The total number of animals counted in all the three independent trials is shown in the parentheses.

Table S3: *spg-7(ad2249)* animals grown on Δ*fes-722* mutant mixed with Live wildtype *E. coli* BW25113 does not arrest as L1-larvae.

Data from three independent trials were collected; the average of percentage of L1 animals and the standard deviation are shown. The total number of animals counted in all the three independent trials is shown in the parentheses.

Table S4: Measurement of CFU/ml of wildtype *E. coli* BW25113 and *E. coli Δfes-722::Kan* in NGM plates

Table S5: Table showing the *spg-7(ad2249)*, *nduf-7(et19)*, *isp-1(qm150)*, *clk-1(qm30)* tested on N-Acetyl Cysteine antioxidant for suppression of arrest phenotype

Data from three independent trials were collected; the average of percentage of L1 animals and the standard deviation are shown. The total number of animals counted in all the three independent trials is shown in the parentheses.

Table S6: Trans-resveratrol treatment acts through antagonizing animal ROS pathways

spg-7(ad2249) animals grown on Δ*fes-722* mutant grown in trans-resveratrol arrest do not arrest while animals grown on Δ*fes-722* mutant *E. coli* pre-grown in the presence of trans-resveratrol and washed to remove trans-resveratrol arrest as L1-larvae.

Supplemental Materials and methods

***C.elegans* strains used in this study**

Strain Name	Description
	N2
SJ4100	*zcIs13[hsp-6::GFP]*
SJ4058	*zcIs9[hsp-60::GFP]*
SJ4005	*zcIs4 [hsp-4::GFP] V*
AU133	*agIs17 [myo-2p::mCherry + irg-1p::GFP] IV*
YL162	*atfs-1(tm4525); zcIs9[hsp-60::GFP]*
QC115	*atfs-1(et15) V*
DA2249	*spg-7 (ad2249) I*
MQ130	*clk-1(qm30) III*
CW152	*gas-1(fc21) X*
MQ887	*isp-1(qm150) IV*
TK22	*mev-1(kn1) III*
CU5991	*fzo-1(tm1133)*
CU6372	*drp-1(tm1108)*
QC134	*nduf-7(et19)*
VC1789	*nduf-2.2(ok2397)*
MQ1333	*nuo-6(qm200)*
NL1832	*ucr-2.3(pk732)*

Genomewide keio screen for developmental delay or *hsp-6::gfp* induction phenotype

Keio mutants which represent ~3800 genes were grown in LB media containing kanamycin at 37°C overnight. 100µl of the overnight culture were dropped onto NGM media containing 24-well plates and grown overnight at 37°C. Synchronized L1-stage transgenic *hsp-6::gfp* animals prepared by bleach-prep were dropped onto these 24-well Keio mutant in NGM media plates. The wells were screened visually at day 3 under a fluorescent microscope for the induction of *hsp-6::gfp*. All the wells were screened visually

at day 5 under the DIC microscope for wells that contained animals growing significantly slower compared to control wells grown on wildtype BW25113 *E. coli*.

The primary hits were rescreened again at least three times.

Removal of Kanamycin cassette in Δ*fes::Kan* Keio mutant and construction of double mutants

Because bacterial insertion drug resistant cassette mutations in one gene in an operon are expected to be polar on downstream genes, the drug resistant cassette alleles are best for identifying relevant operons rather than individual genes. But because genes in operons often act in the same pathway, the identification of the operon is informative (Table S1). Mutations that disrupt the *E. coli* cytochrome oxidase *cyoABCDE* operon were previously shown to induce *C. elegans hsp-6:GFP* (Govindan et al., 2015b) ; these were among the strongest hits of the 24 mutants that caused developmental delay (Table 1). None of the other *E. coli* genes identified in the screen of the Keio mutant collection act in the *E. coli* electron transport chain, consistent with our previous finding that inactivation of only specific steps in bacterial respiration causes defects in *C. elegans* growth or mitochondrial function (Govindan et al., 2015b). Keio mutants have a Kanamycin cassette flanked by FLP recombinase sites, which allows for the excision of the cassette in the place of gene of interest (Baba et al., 2006). Kanamycin cassette incision in *Δfes::Kan* was achieved by introducing the plasmid pCP20 by transformation, which contains an Flp recombinase. Transformants were selected for ampicillin resistance at 30°C and the raised at 42°C to remove the pCP20 plasmid. Colonies were verified by inability to grow on LB plates with Kanamycin as well as by sequencing for the recombination site junction.

Double mutants, *Δfes entA::kan*, *Δfes entB::kan*, *Δfes cirA::kan*, *Δfes fiu::kan*, or *Δfes fepA::kan* were generated as follows: P1 lysates of Keio collection mutants, *entA::kan*, *entB::kan*, *cirA::kan*, *fiu::kan*, or *fepA::kan* strains were generated by growing overnight cultures of each strain in LB media containing 2mM $MgSO_4$,10mM $CaCl_2$, 0.2% glucose at 37°C until the OD_{600} is around 0.5. 100 µl of Phage P1 obtained form CGSC was added to 1 ml of each culture. After 2 hours incubation at 37°C until complete lysis, 0.5 ml of chloroform was added the culture. The lysates were centrifuged at 13K RPM for 1 min and the lysates were stored in 4°C until use. 100 µl of P1 lysate from each of the Keio mutant was

added to overnight cultures of *Δfes* mutants grown in LB was suspended in 1ml LB media containing 5mM $MgSO_4$, 50mM $CaCl_2$ and incubated at 37°C for 1 hour. 0.5 ml of 10mM Sodium citrate was added to each tube and incubated for 30 min. The tubes were centrifuged at maximal speed for 1 min and plated on kanamycin containing LB Media agar plates. The colonies were verified for the presence of *Δfes* and Keio mutant insertions using sequencing.

***In vitro* ATP measurement**

ATP measurements were conducted as per the protocol with the following modifications (Palikaras and Tavernarakis, 2016). 1000 animals in 100 µl of M9 were frozen in liquid nitrogen and stored at -80°C until analysis. The samples were placed immediately in boiling water bath for 15 min. After adding twice amount of distilled water, centrifugation was done at 14,000 rpm for 5 min and supernatant is transferred into a second tube. Equal volume of luciferase reagent (Promega^{TM}) was added and luminescence was measured using a plate reader (SpectraMax Microplate reader). Protein content was measured using BCA method. ATP concentrations were normalized to protein content of samples. All the values were normalized to wildtype grown on *E. coli* BW25113.

***In vivo* ATP measurement**

The transgenic reporter strain PE254 *(feIs4[Psur-5::luc+::gfp; rol-6 (su1006)] V)* (Lagido et al., 2015) was used as a surrogate for determining the intracellular ATP content. ~1000 synchronized PE254 animals grown in *E. coli* BW25113 or *Δfes* mutant until the L4-larval stage were collected from NGM media plates and washed at least 4 times in M9 buffer to remove bacteria. The animals were transferred to white flat-bottom, 96-well plate wells containing 100 µM D-luciferin in M9 buffer and the luminescence was measured within 5 min in SpectraMax microplate reader. GFP fluorescence was quantified in SpectraMax microplate reader using 485nm excitation and a 520nm emission filter. Background measurements were subtracted from readings. Luminescence values were normalized to GFP fluorescence of samples. All the values were normalized to wildtype grown on *E. coli* BW25113.

Measuring endogenous hydrogen peroxide levels using HyPer strain

To measure endogenous hydrogen peroxide levels, transgenic *jrIs1*[P*rpl-17*::HyPer] animals expressing a HyPer as described (Back et al., 2012b). Synchronized L1-stage transgenic *jrIs1*[P*rpl-17*::HyPer]

animals were grown in *E. coli* BW25113 or *Δfes* mutant and about 1000 L4-stage animals were harvested in 96 microtiter well plates. For H_2O_2 treatment experiment, H_2O_2 was added to the animals in the 96-well itself and measurements were taken within 15 minutes. An excitation wavelength of either 490 nm or 405 nm was used to measure oxidized or reduced HyPer probe fluorescence respectively with an emission filter of 535 nm. The absorbance at 620 nm was used to normalize for animal numbers. The statistical significance of differences between conditions was determined by using unpaired *t*-test. GraphPad Prism 8.0 was used for these calculations.

Staining of mitochondria

Animals were stained with 10μM of 10-nonyl acridine orange bromide (NAO) in M9 solution for 1 hour and destained by washing in M9 atleast 5 times.

Antioxidant treatments

Stock solutions of trans-resveratrol, L-ascorbic acid, cis-resveratrol, oxyresveratrol, cis-trimethoxyresveratrol, trolox, or N-acetyl cysteine were diluted in M9 to a working concentration of 10μg/ml and dropped onto NGM media plates seeded with overnight cultures of *Δfes* mutant *E. coli*. Synchronized L1-stage *spg-7(ad2249)* animals were added to the plates and scored after three days for the suppression of arrest phenotype. The negative control NGM plates contained the solvent and M9.

Microscopy and imaging

Nematodes were mounted onto agar pads and images were taken using a Zeiss AXIO Imager Z1 microscope fitted with a Zeiss AxioCam HRm camera and Axiovision 4.6 (Zeiss) software. Student's t test was used determine statistical significance.

Low-magnification bright-field images were acquired using a Zeiss AxioZoom V16 Microscopre, equipped with a Hammamatsu Orca flash 4.0 digital camera camera, and using Axiovision software. Some Immunofluorescence images were acquired with an IX-70 microscope (Olympus, Waltham, MA) fitted with a cooled CCD camera (CH350; Roper Scientific) driven by the Delta Vision system (Applied Precision, Pittsburgh, PA). Images were deconvolved using the SoftWoRx 3.3.6 software (Applied Precision).

Quantification and Statistical analysis

Statistical analysis was performed with GraphPad Prism 7 software. Student's t-test was used for analysis.

Reference:

Baba, T., Ara, T., Hasegawa, M., Takai, Y., Okumura, Y., Baba, M., Datsenko, K.A., Tomita, M., Wanner, B.L., Mori, H., 2006. Construction of Escherichia coli K-12 in-frame, single-gene knockout mutants: the Keio collection. Mol Syst Biol 2, 2006–0008. doi:10.1038/msb4100050

Back, P., De Vos, W.H., Depuydt, G.G., Matthijssens, F., Vanfleteren, J.R., Braeckman, B.P., 2012. Exploring real-time in vivo redox biology of developing and aging Caenorhabditis elegans. Free Radic. Biol. Med. 52, 850–859. doi:10.1016/j.freeradbiomed.2011.11.037

Govindan, J.A., Jayamani, E., Zhang, X., Mylonakis, E., Ruvkun, G., 2015b. Dialogue between E. coli free radical pathways and the mitochondria of C. elegans. Proc Natl Acad Sci U S A. doi:10.1073/pnas.1517448112

Lagido, C., McLaggan, D., Glover, L.A., 2015. A Screenable In Vivo Assay for Mitochondrial Modulators Using Transgenic Bioluminescent Caenorhabditis elegans. J Vis Exp e53083–e53083. doi:10.3791/53083

Palikaras, K., Tavernarakis, N., 2016. Intracellular Assessment of ATP Levels in Caenorhabditis elegans. Bio Protoc 6. doi:10.21769/BioProtoc.2048

Table 1

	Wildtype *C. elegans* animals		***spg-7(ad2249)* mutant**	
	% Adults		**% Adults**	
***E. coli* genotype**	**Day 3**	**Day 4**	**Day 4**	**Day 5**
BW25113 (Wildtype)	100±0 (244)	NA	100±0 (195)	ND
fes	100±0 (244)	NA	0±0 (169)	0±0 (224), **L1-arrest**
fepG	100±0 (265)	NA	0±0 (185)	0±0 (246), **L1-arrest**
fepD	100±0 (259)	NA	0±0 (183)	0±0 (255), **L1-arrest**
fepC	100±0 (214)	NA	0±0 (186)	0±0 (247), **L1-arrest**
cyoD	9.8±3.7 (221)[a,b]	83.2±9 (236)	0±0 (181)	64.6±6.4 (244)
yafC	100±0 (240)	NA	0±0 (167)	60.6±8 (256)
cyoB	0±0 (233)[b]	59±6.3 (233)	0±0 (188)	66.6±7.2 (247)
cyoA	0±0 (256)[b]	69.4±17.2(227)	0±0 (155)	77.1±5 (235)
tap	83±6.4 (251) [a]	98.2±0.8(238)	0±0 (166)	78.3±20 (226)
cpxR	0±0 (249)[b]	69.2±15.4 (233)	0±0 (185)	80.7±13.4 (235)
stfP	0±0 (255)[b]	64±8.4 (248)	0±0 (149)	74.6±10.9 (250)
mdoC	0±0 (247)[b]	72.2±11.7 (229)	0±0 (156)	75.1±9.1 (215)
ycfk	0±0 (233)[b]	72.9±17.4 (221)	0±0 (181)	78.7±7.7 (208)
yejL	100±0 (260)	NA	0±0 (209)	76.4±12.3 (260)
yejK	100±0 (210)	NA	0±0 (182)	80.3±6.4 (228)
allA	0±0 (233)[b]	52.8±14.1 (241)	0±0 (172)	81.8±4.6 (236)
ybjX	0±0 (197)[b]	56.9±15.4 (230)	0±0 (178)	71.5±14.8 (225)
yfaE	0±0 (250)[b]	55.1±13.2 (240)	0±0 (184)	82.6±3.8 (236)
ybaW	0±0 (246)[b]	63.1±9.5 (255)	0±0 (192)	80.1±8 (237)
ycfX	0±0 (240)[b]	62.9±8.9 (257)	0±0 (192)	82.4±10.3 (234)
ygbM	0±0 (187)[b]	61.4±12.8 (230)	0±0 (200)	69±5.5 (224)
ydaN	0±0 (260)[b]	63.1±7.9 (232)	0±0 (194)	79.1±1.6 (220)
ybiB	0±0 (243)[b]	57.1±15.5 (236)	0±0 (199)	76.7±5.9 (227)
mntR	100±0 (264)	NA	0±0 (135)	76.9±9.8 (219)
yaaJ	100±0 (228)	NA	0±0 (159)	66.2±16.4 (231)
yfaY	0±0 (253)[b]	61.7±15.6 (245)	0±0 (188)	73±18 (247)
yejB	0±0 (228)[b]	60.2±3.7 (251)	0±0 (172)	66.4±12.2 (233)
yfiB	0±0 (234)[b]	59.8±3.6 (250)	0±0 (190)	75.1±8.1 (233)
tar	100±0 (242)	NA	0±0 (179)	73.9±4 (226)
yheT	0±0 (252)[b]	64.6±4.7 (234)	0±0 (154)	77.7±7.5 (233)
yaaU	100±0 (257)	NA	0±0 (196)	80.4±7.1 (251)
aroH	100±0 (231)	NA	0±0 (172)	76.8±4 (235)
aes	0±0 (232)[b]	63.9±5.3 (239)	0±0 (181)	76.3±2.1 (234)
cyaA	100±0 (257)	NA	0±0 (165)	77.6±2(223)
hlyE	100±0 (227)	NA	0±0 (159)	75.1±3.4 (237)
yceF	0±0 (238)[b]	72.47±3.1 (236)	0±0 (193)	78.2±2 (252)
wbbI	0±0 (236)[b]	63.5±8.8 (239)	0±0 (183)	69.7±12 (253)
ssuE	100±0 (244)	NA	0±0 (195)	77±6.5 (232)
cspH	100±0 (270)	NA	0±0 (163)	71±6.6 (230)
yaiF	100±0 (251)	NA	0±0 (198)	75.5±6.4 (236)
rhsD	100±0 (255)	NA	0±0 (169)	82.6±0.65(236)
rhsB	100±0 (265)	NA	0±0 (182)	80.4±5.2 (244)
ydcC	0±0 (240)[b]	67.7±15.7 (239)	0±0 (183)	67.7±13.2 (246)
cspD	100±0 (215)	NA	0±0 (137)	77.8±7.4 (229)
eutD	100±0 (256)	NA	0±0 (165)	78.4±4.6 (242)

Table 2

Fed on	Description	% Larval arrest (N)	
		Wildtype	***spg-7(ad2249)***
BW25113	Wildtype	0±0 (179)	0±0 (219)
ΔfepC726::kan	*Ferric enterobactin transport; ATP-binding protein fepC*	0±0 (132)	100±0 (178)
ΔfepG727::kan	*Ferric enterobactin transport system permease protein FepG*	0±0 (195)	100±0 (196)
ΔfepD728::kan	*Ferric enterobactin transport system permease protein FepD*	0±0 (198)	100±0 (181)
ΔfepB730::kan	*Ferrienterobactin-binding periplasmic protein*	0±0 (231)	0±0 (174)
ΔfepA721::kan	*Ferrienterobactin receptor*	0±0 (159)	0±0 (188)
Δfiu-777::kan	*Catecholate siderophore receptor Fiu*	0±0 (188)	0±0 (164)
ΔcirA782::kan	*Colicin I receptor; Postulated to participate in iron transport*	0±0 (201)	0±0 (190)
Δfes-722::kan	*Enterochelin esterase*	0±0 (151)	100±0 (205)
ΔentF724::kan	*Enterobactin synthase component F*	0±0 (142)	0±0 (165)
ΔentC731::kan	*Isochorismate synthase EntC*	0±0 (166)	0±0 (179)
ΔentE732::kan	*Enterobactin synthase component E*	0±0 (202)	0±0 (173)
ΔentB733::kan	*Enterobactin synthase component B*	0±0 (191)	0±0 (172)
ΔentA734::kan	*2,3-dihydro-2,3-dihydroxybenzoate dehydrogenase*	0±0 (183)	0±0 (162)

Table 3

		% Larval arrest (N)	
Animal Strain	**Description**	**Fed on BW25113**	**Fed on *Δfes-722***
Wildtype		0±0 (130)	0±0 (115)
fzo-1(tm1133)	Mitofusin/FZO1	0±0 (80)	0±0 (95)
drp-1(tm1108)	Dynamin related protein1 (DRP1)	0±0 (77)	0±0 (93)
nduf-7(et19)	NADH dehydrogenase [ubiquinone] Fe-S Protein 7 (NDUF7) of Complex I mutated in Leigh syndrome	0.7±1.2 (88)	99.2±1.2 (147)
gas-1(fc21)	NADH dehydrogenase [ubiquinone] Fe-S Protein 2 (NDUF2) of Complex I	0.5±0.9 (101)	0±0 (119)
nduf-2.2(ok2397)	NADH dehydrogenase [ubiquinone] Fe-S Protein 2 (NDUF2) of Complex I	0±0 (100)	0±0 (120)
nuo-6(qm200)	NADH dehydrogenase [ubiquinone] 1 beta subcomplex subunit 4 (NDUFB4/B15) of Complex I	0±0 (98)	0±0 (99)
mev-1(kn1)	Succinate Dehydrogenase subunit (SDHC-1) of complex II	0±0 (96)	0±0 (81)
isp-1(qm150)	Ubiquinol-cytochrome C reductase, Rieske Fe-S protein (UQCRFS1) of complex III	1.2±1.1 (92)	100±0 (166)
ucr-2.3(pk732)	Ubiquinol-cytochrome C reductase core protein 2 (UQCRC2) of Complex III.	0±0 (99)	0±0 (95)
clk-1(qm30)	COQ7; Essential for Ubiquinone biosynthesis	0±0 (94)	100±0 (128)

Figure 1

A

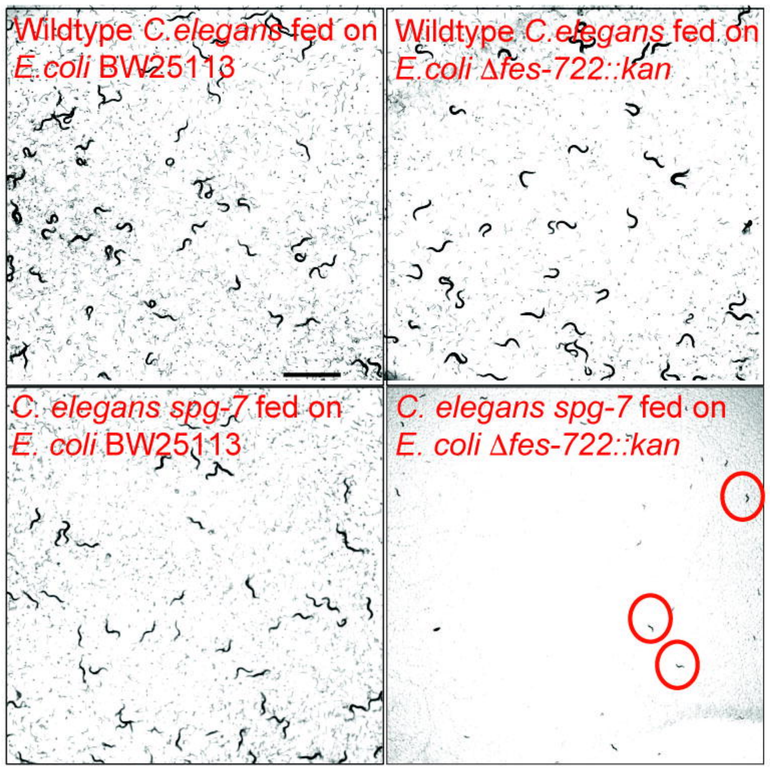

B

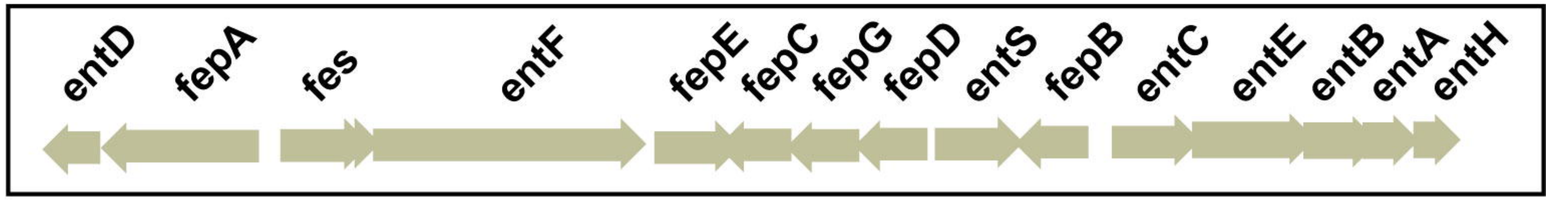

C

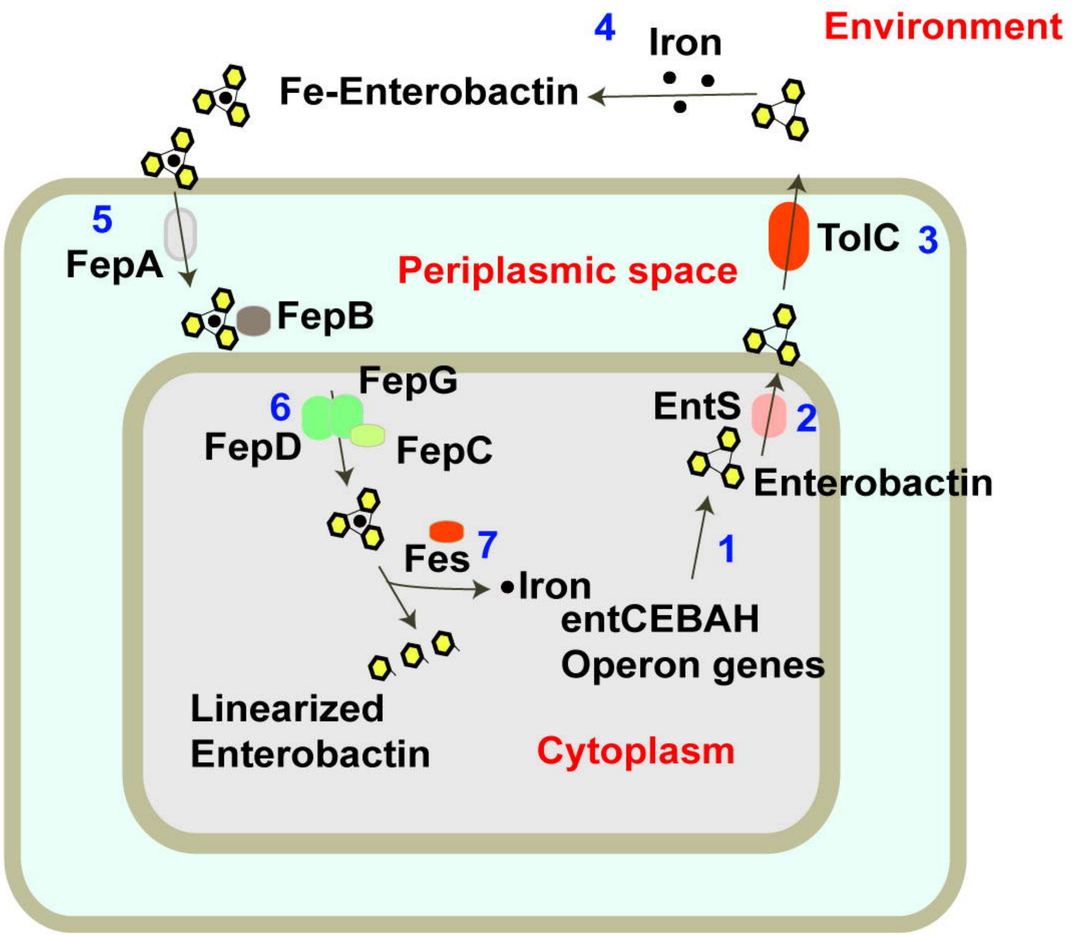

E. coli

Figure 2

A

***C. elegans spg-7* fed on *E. coli* BW25113**

C. elegans spg-7* fed on *E. coli* Δ*fes-722

C. elegans spg-7* fed on *E. coli* Δ*fes-722* Δ*entA734

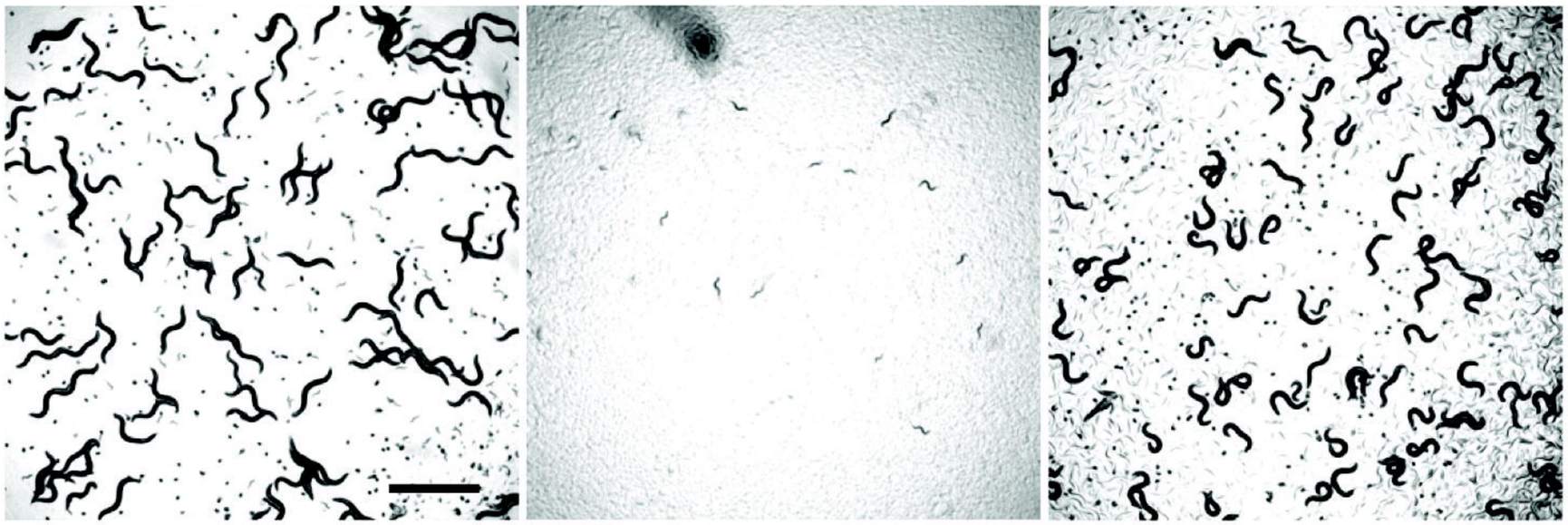

B

	% Larval arrest (N)
Fed on *E. coli*	***C. elegans spg-7***
BW25113	0±0(142)
Δfes	100±0(140)
Δfes ΔentB::kan	0±0(144)
Δfes ΔentA::kan	0±0(153)
Δfes ΔcirA::kan	100±0(134)
Δfes Δfiu::kan	100±0(136)
Δfes ΔfepA::kan	0±0(146)

Figure 3

A

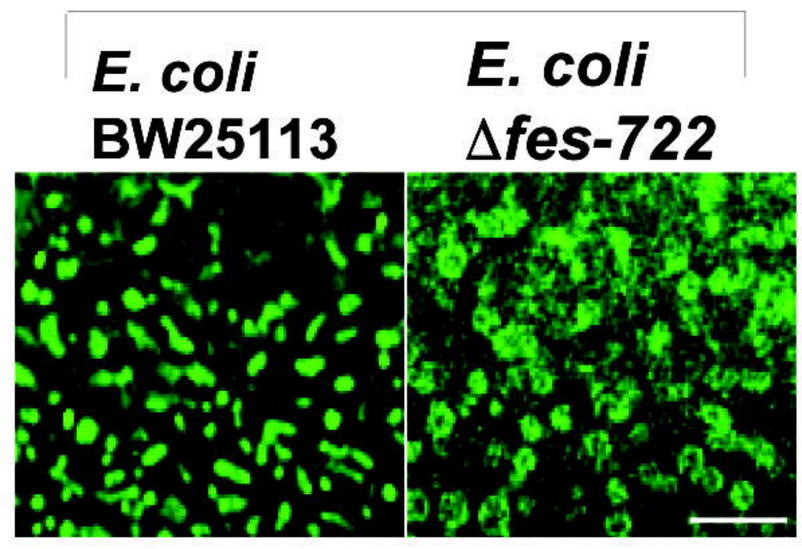

B

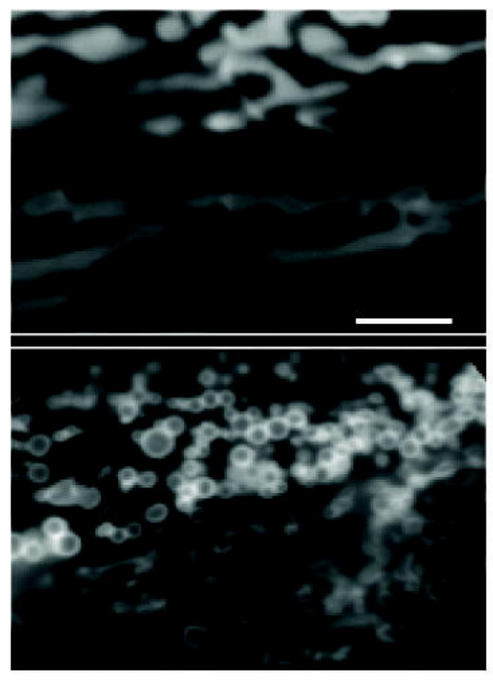

C

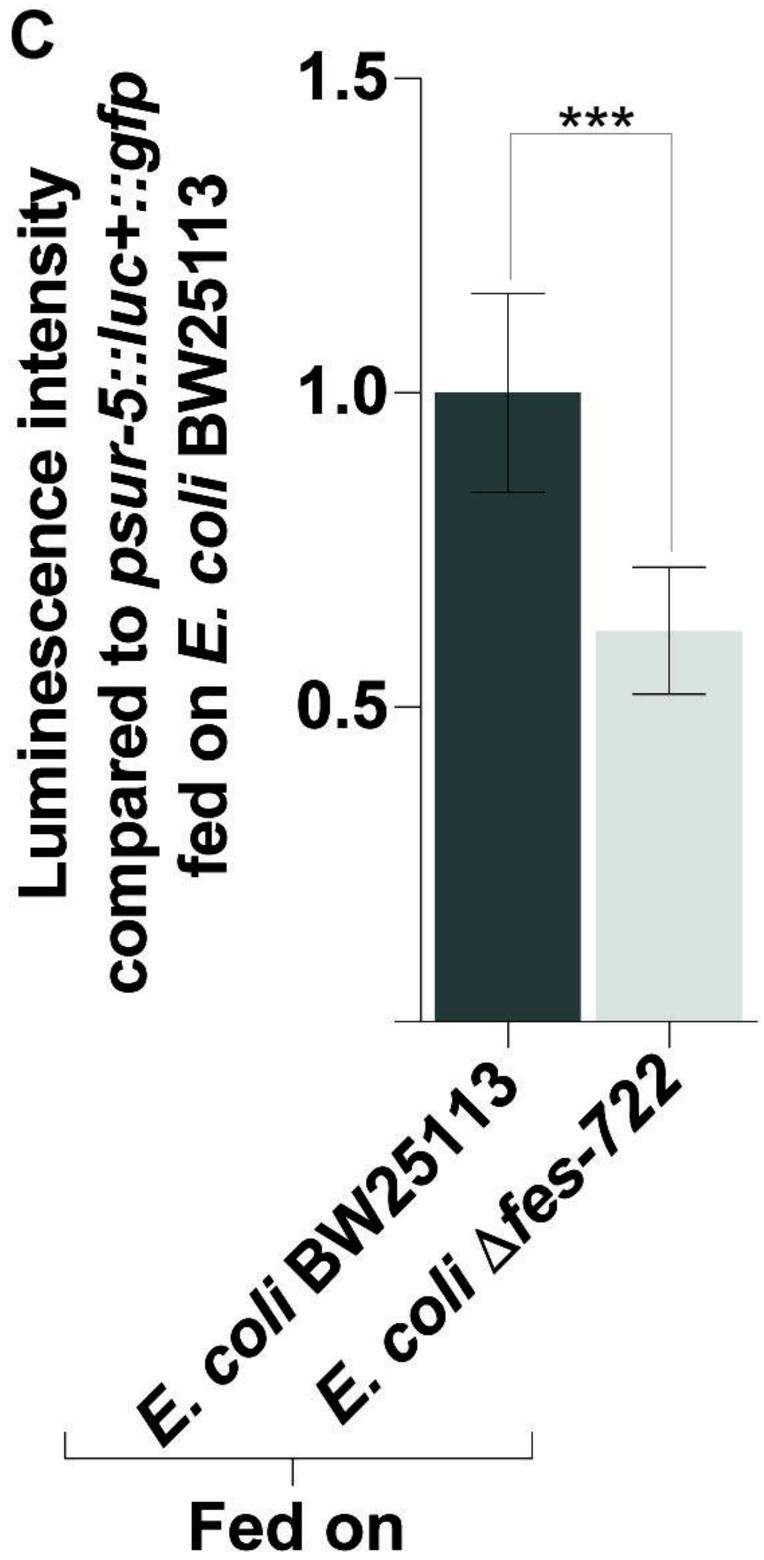

D

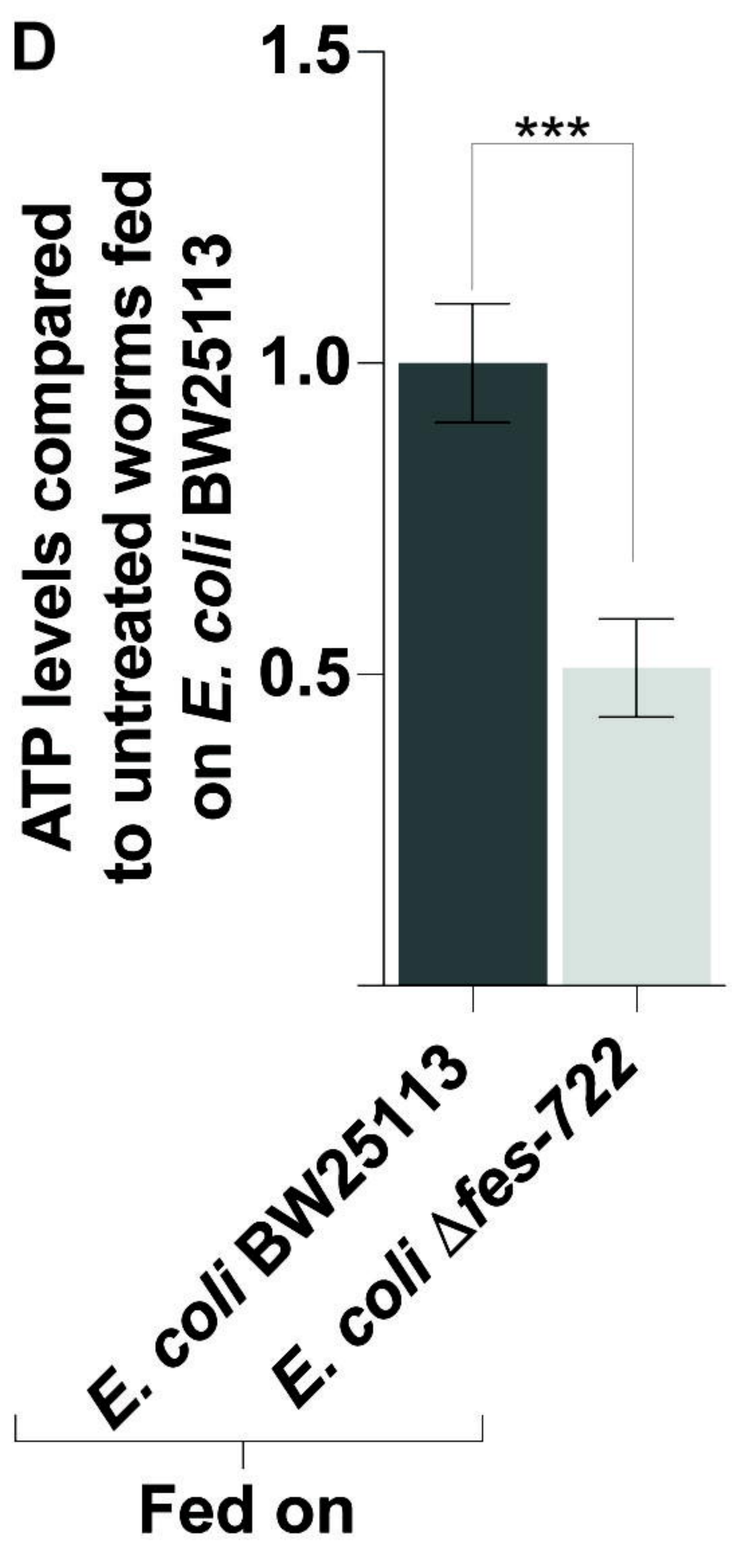

E

C. elegans spg-7 fed on *E. coli Δfes-722*	% Larval arrest (N)
solvent control	100±0(118)
Trans-Resveratrol, 10μg/ml	1.4±1.2(144)
L-Ascorbic acid, 10μg/ml	0±0(136)
Cis-Resveratrol, 10μg/ml	100±0(146)
Oxyresveratrol, 10μg/ml	2.7±3.1(143)
Cis-trimethoxyresveratrol, 10μg/ml	100±0(140)
Trolox, 10μg/ml	0±0(141)
N-acetyl cysteine, 10μg/ml	0±0(147)

F

C. elegans spg-7 fed on *Δfes-722*, treated with	% Larval arrest (N)
solvent control	100±0(181)
rLipocalin, 0.4μM	0.5±0.9(193)